Supporting information

Ligand-triggered Electrostatic Self-assembly of CdS nanosheets/Au Nanocrystals Nanocomposites for Versatile Photocatalytic Redox Applications

Qingchi Xu[a*], Jiaxin Zeng[a], Haiqing Wang[a], Xingyun Li[a], Jun Xu[a], Jianyang Wu[a], Guangcan Xiao[b], Fang-Xing Xiao[b*], Xiangyang Liu[ca]

[a] Department of Physics, Research Institute for Biomimetics and Soft Matter, Fujian Provincial Key Laboratory for Soft Functional Materials, Xiamen University, Xiamen, 361005, P. R. China.

[b] Instrumental Measurement and Analysis Center, Fuzhou University, Fuzhou, People's Republic of China.

[c] Department of Physics, National University of Singapore, 2 Science Drive 3, Singapore, 117542, Singapore.

Email: xuqingchi@xmu.edu.cn
fangxing2010@gmail.com

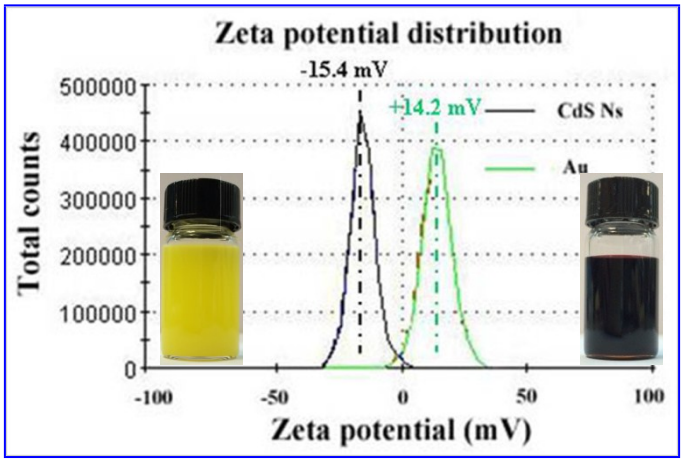

Fig. S1. Zeta potential of CdS Ns@*L*-cysteine and Au@DMAP NPs aqueous suspensions.

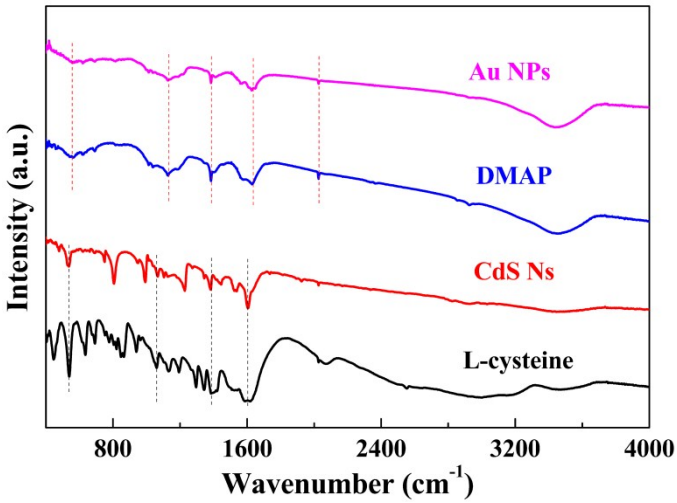

Fig. S2. FTIR spectra of *L*-cysteine, CdS Ns, DMAP and Au@DMAP NPs.

Note: Fig. S2 shows the FTIR spectra of *L*-cysteine, CdS Ns, DMAP and Au@DMAP NPs. Noteworthily, the characteristic peaks at 556, 1132, 1388 and 2030 cm^{-1} in the FTIR spectrum of Au@DMAP NPs are attributed to the functional groups of DMAP ligand, which is in faithful agreement with FTIR spectrum of pure DMAP, indicating DMAP has been successfully attached on the surface of Au NPs. Similarly, the featured peaks at 536, 1061, 1395 and 1611 cm^{-1} in the FTIR spectrum of CdS Ns can be accurately assigned to the functional groups of *L*-cysteine, which also agrees well with FTIR spectrum of pure *L*-cysteine, suggesting that *L*-cysteine has also been successfully tethered on the CdS Ns surface.

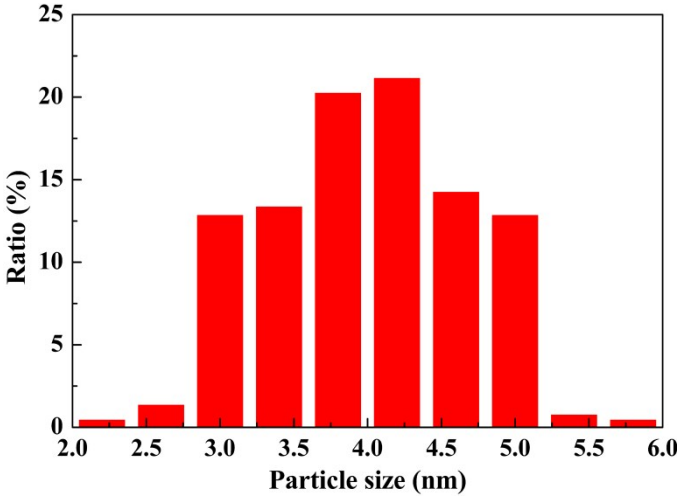

Fig. S3. Size distribution of Au@DMAP NPs (217 nanoparticles counted).

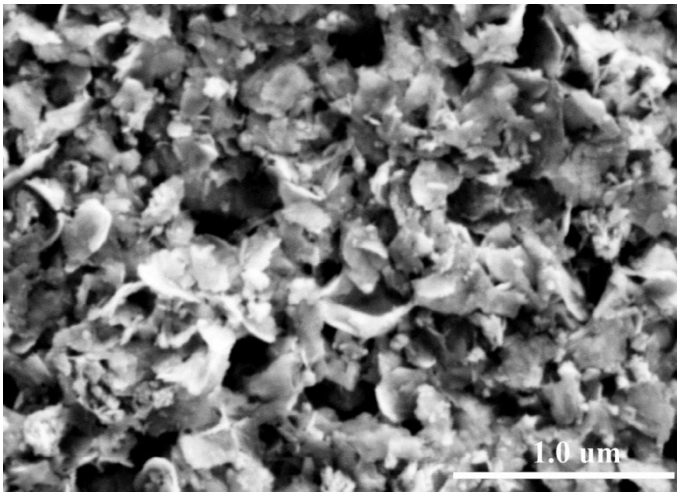

Fig. S4. FESEM image of CdS Ns.

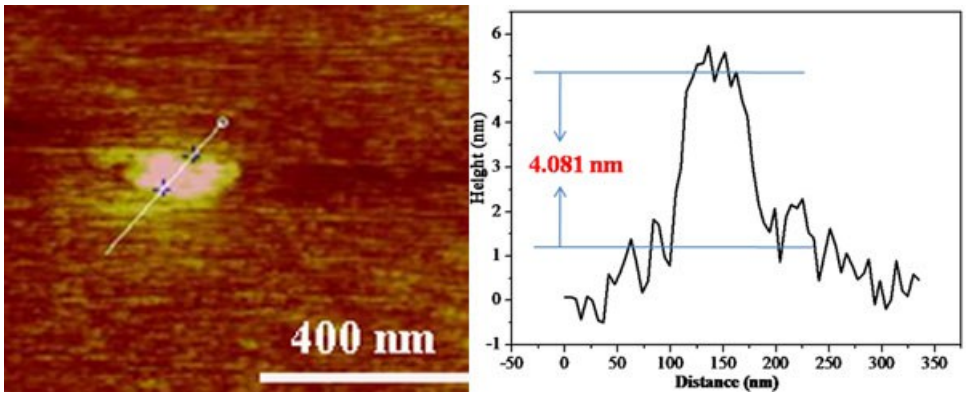

Fig. S5. Representative AFM image and corresponding thickness analysis of CdS Ns

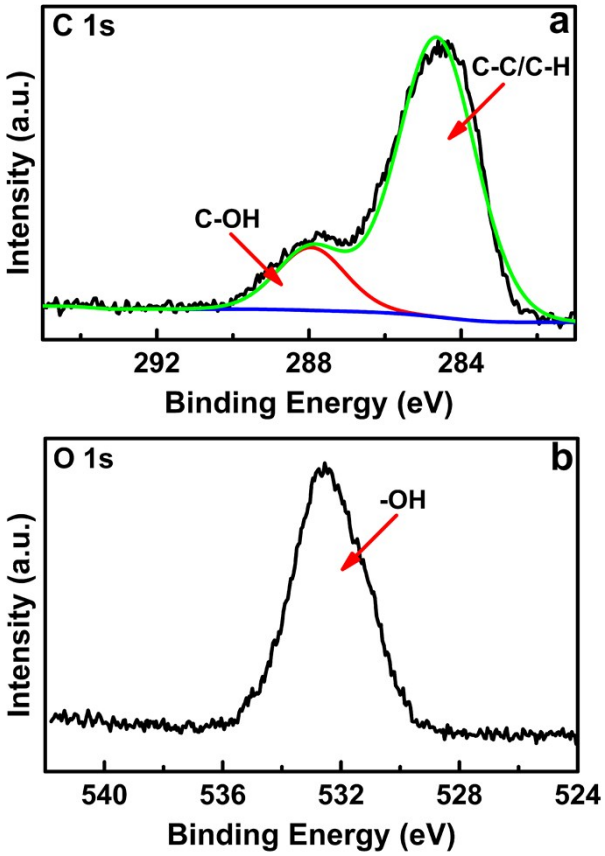

Fig. S6. High-resolution XPS spectra of C 1s and O 1s for 1Au-CdS Ns nanocomposite.

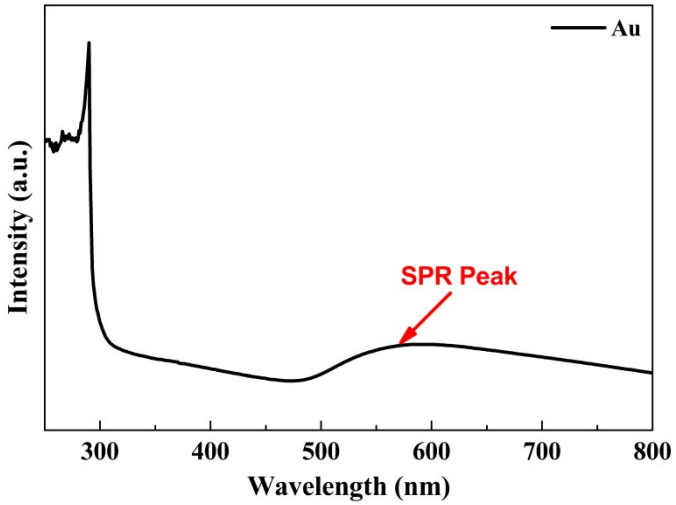

Fig. S7. UV-absorption spectrum of Au@DMAP NPs aqueous suspension.

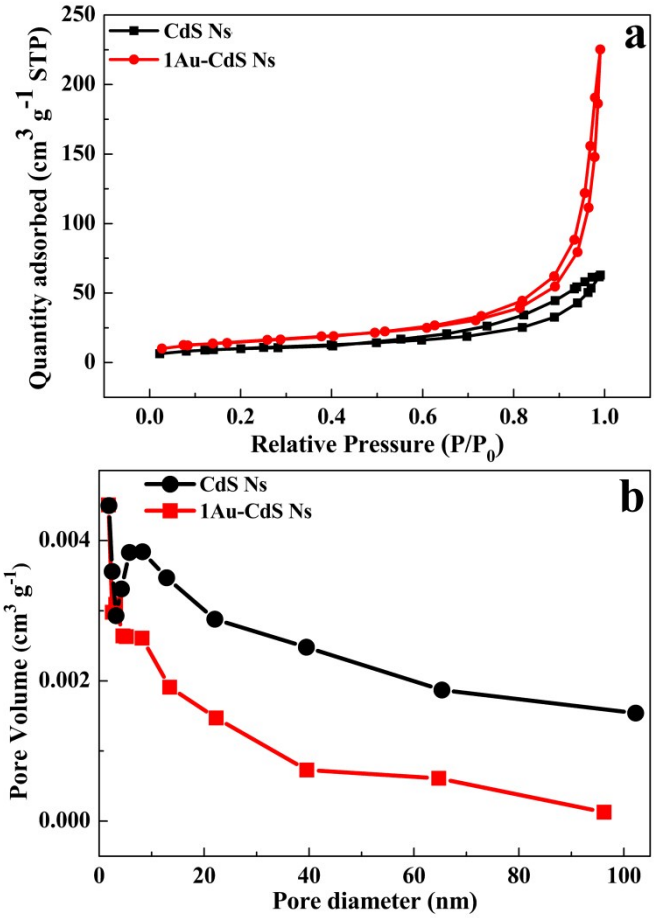

Fig. S8. (a) N_2 adsorption-desorption isotherms and (b) pore size distribution of CdS Ns and 1Au-CdS Ns nanocomposite.

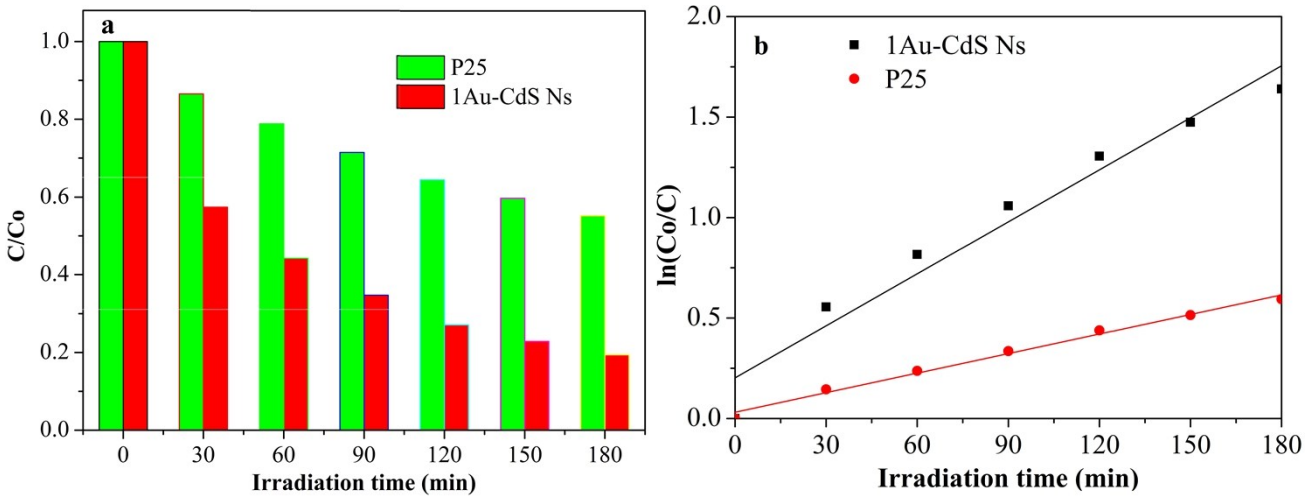

Fig. S9. (a) Photocatalytic activities of P25 and 1Au-CdS Ns for degradation of MB under visible light irradiation ($\lambda \geq 420$ nm) at ambient conditions with corresponding kinetic fitting curves displayed in (b).

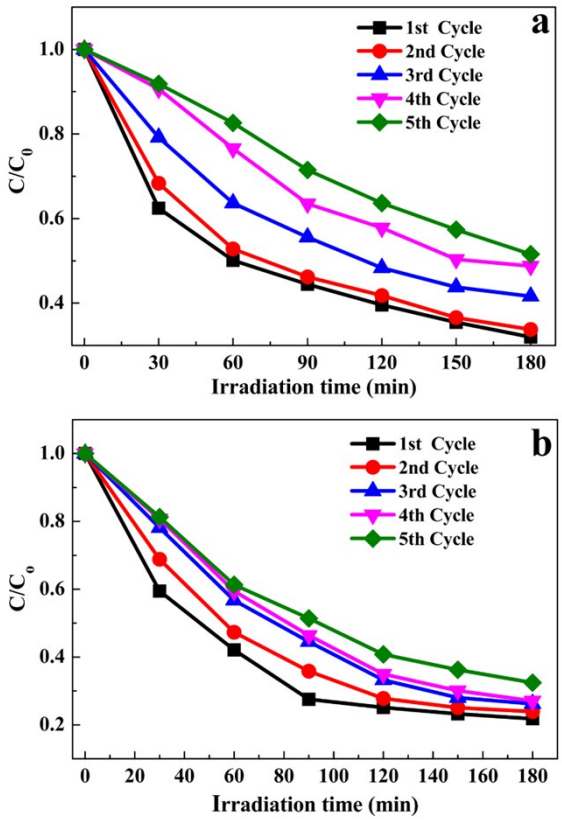

Fig. S10. Photocatalytic activities of (a) CdS Ns and (b) 1Au-CdS Ns nanocomposite for five successive cycling experiments toward degradation of MB under visible light irradiation ($\lambda \geq 420$ nm).

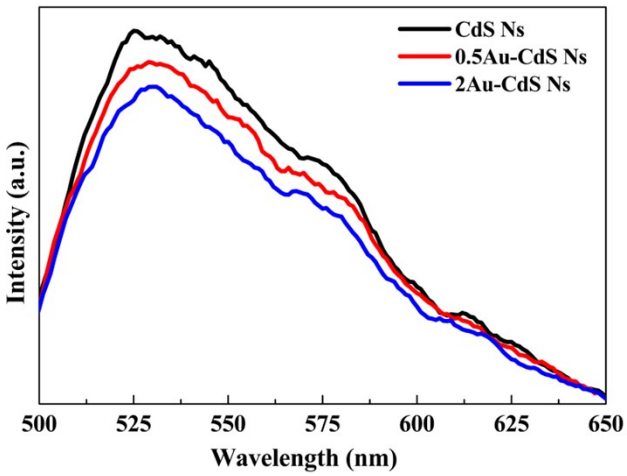

Fig. S11. PL results of CdS Ns and Au- CdS Ns nanocomposites.

Note: Au-CdS Ns nanocomposites (0.5 and 2 %) demonstrated decreased PL intensity in comparison with CdS Ns, indicating Au NPs are beneficial for trapping photoelelctrons leading to prolonged lifetime of photogenerated charge carriers in nanocomposites.

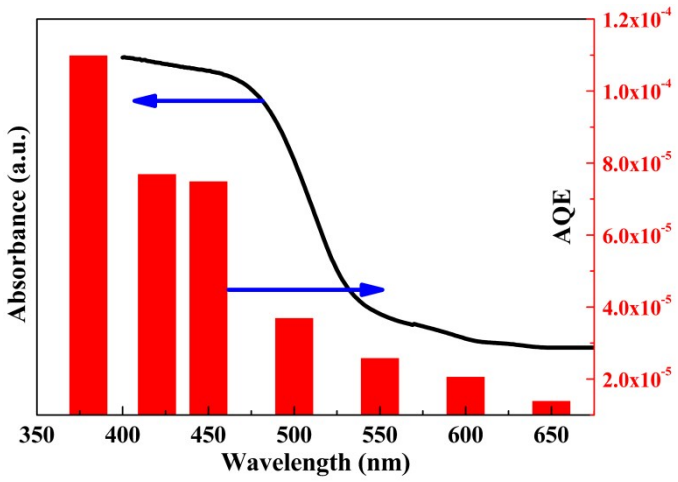

Fig. S12. AQE curve (right axis) with corresponding UV-Vis diffuse reflectance spectrum (left axis) of CdS Ns.

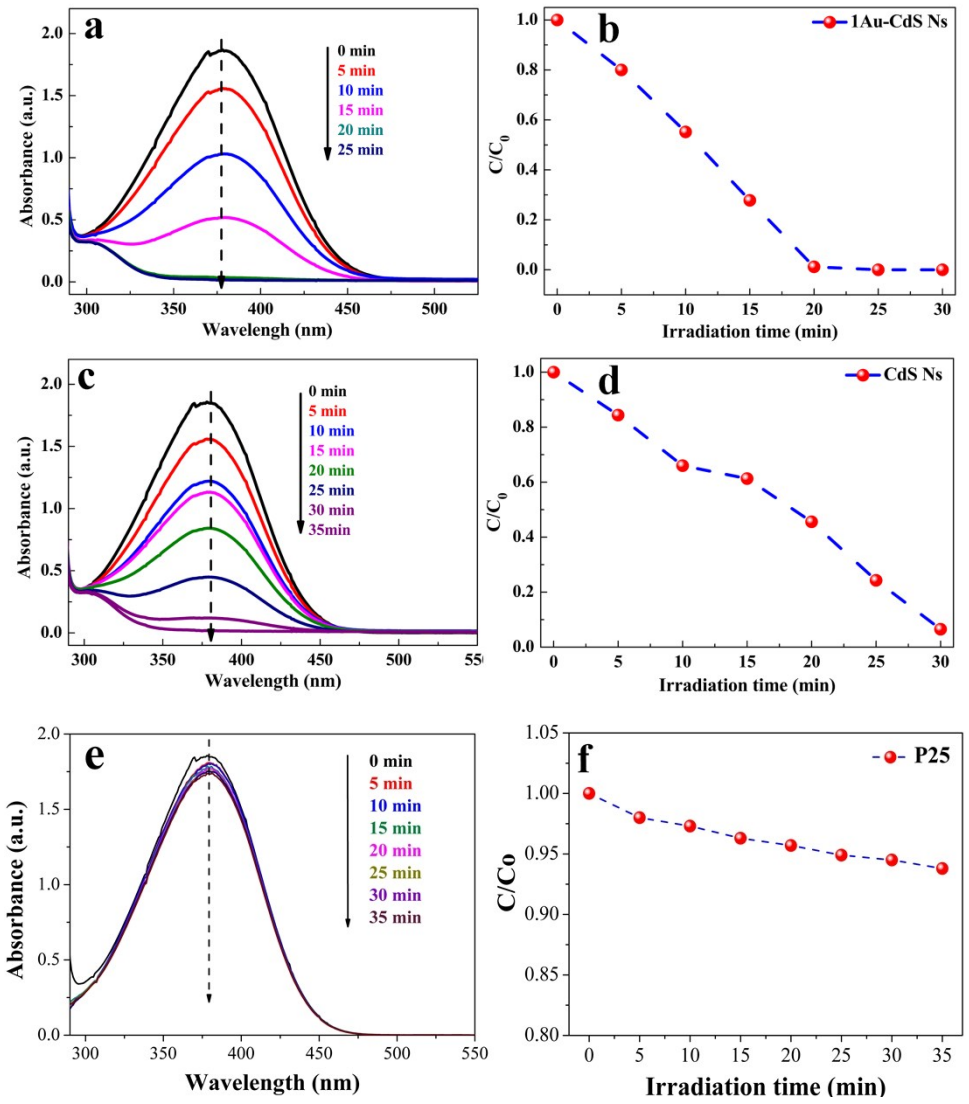

Fig. S13. Time-dependent variations in the UV absorbance spectra of 4-NA catalyzed by (a) 1Au-

CdS Ns, (c) CdS Ns nanocomposite and (e) P25 as a function of visible light irradiation time; Photocatalytic performances of (b) 1Au-CdS Ns, (d) CdS Ns nanocomposite and (f) P25 toward reduction of 4-NA as a function of visible light irradiation time.